Geothermics 48 (2013) 80–92

Contents lists available at ScienceDirect

Geothermics

journal homepage: www.elsevier.com/locate/geothermics

Optimization of injection scheduling in fractured geothermal reservoirs

Egill Juliusson*, Roland N. Horne

Stanford University, Department of Energy Resources Engineering, 367 Panama Street, Green Earth Sciences 065, Stanford, CA 94305, USA

ARTICLE INFO

Article history:
Received 25 June 2012
Accepted 1 May 2013
Available online 27 July 2013

Keywords:
Geothermal
Optimization
Injection
Interwell connectivity
Tracer transport
Thermal transport
Thermal breakthrough
Power output
Fractures
Enhanced geothermal systems

ABSTRACT

This article describes a method for optimizing injection rates in fractured geothermal reservoirs. The optimization approach suggested here is based on maximizing the net present value (NPV) of production revenue from the reservoir. The method relies on tracer and flow-rate data, which are used to calibrate a thermal transport model in such a way that the thermal drawdown depends on the injection rates. Then, an empirical correlation is used to relate the injection and production temperature to the specific electrical power output. The power output model, in conjunction with predictions for the future energy prices and interest rates, allows the computation of the NPV as a function of the injection rates. This characterization of the problem makes it possible to solve it quickly and efficiently.

The optimization method was applied to two discrete-fracture reservoir simulation models. The first having a relatively simple structure with two injectors and two producers and the second being a more complex model with seven wells and a fracture structure based on observations from the Soultz-sous-Forêts enhanced geothermal system (EGS) in France. The results show that the method works well for both the simple and more complex case. A finding of particular interest is that the optimal injection schedule depends strongly on the minimum design temperature for the power plant.

1. Introduction

Determining how to allocate water to injection wells in geothermal fields is an important and challenging task. Conceptually, the objective with injection scheduling is to delay thermal breakthrough as long as possible, while maintaining as much pressure support for the production wells as possible. For example, one can aim to maximize thermal recovery from the geothermal resource, or maximize the NPV (defined as the net value in the present of a sum of money, in contrast to some future value it will have when it has been invested at compound interest) of production revenue from the reservoir. The same requirement applies to both EGS and conventional hydrothermal resources.

Lovekin and Horne (1989) discussed methods for optimizing injection schedules in geothermal reservoirs based on tracer return data. They posed the problem as both a linear program where only the injection rates were adjusted, and a quadratic program where injection and production rates were adjusted simultaneously. In a linear program both the objective function and the constraints depend linearly on the decision variable whereas in a quadratic program the objective function is quadratic but the constraints are linearly dependent on the decision variable.

The objective functions depended on well-to-well connectivity parameters that were inferred from tracer tests and well locations. These connectivity parameters were computed in an empirical manner and their value was independent of the injection and production rates. Macario (1991) applied this optimization method with tracer and chloride monitoring data from the Palinpinon I field, in the Philippines. Sullera and Horne (2001) later improved upon the analysis of the chloride data using measurements from both Palinpinon I and Dixie Valley, Nevada.

Whether tracer returns vary much with injection and production rates depends on the characteristics of the geothermal reservoir. In cases where the flow-rates being circulated by the power plant are small in comparison to the natural advective flow rate circulating in the reservoir, it seems reasonable to assume that the tracer returns would be insensitive to the particular configuration of injection and production rates. In EGS, on the other hand, the natural advective flow rate is often negligible and thus the tracer returns would vary more significantly with the injection and production rate configuration.

Juliusson (2012) introduced a method for predicting tracer returns under variable flow-rate conditions in fractured geothermal systems. The crux of the method is to view the tracer returns as functions of the cumulative flow from well-to-well, as opposed

* Corresponding author at: Haaleitisbraut 68, 103 Reykjavik, Iceland. Tel.: +354 695 1184.
E-mail address: egill.juliusson@gmail.com (E. Juliusson).

0375-6505/$ – see front matter © 2013 Elsevier Ltd. All rights reserved.
http://dx.doi.org/10.1016/j.geothermics.2013.05.004

Notation

Symbols

A	heat-transfer area of flow path (m^2)
b	effective fracture half aperture (m)
c	concentration (g/m^3)
C	specific heat capacity (J/(kg °C))
F	interwell connectivity based on flow-rate data
$\tilde{F}$	interwell connectivity based on tracer data
K	thermal conductivity (W/(m K))
L	length of fracture or distance between wells (m)
N_I	total number of injection wells in a field (wells)
N_p	total number of injection wells in a field (wells)
n	time-like discrete variable (days)
O	objective function ($)
P	electricity price ($/MWh)
q	flow rate (m^3/day)
Q	cumulative flow (m^3)
r	interest rate (continuous compounding) (%/year)
R	retardation factor
t	time (days)
T	temperature (°C)
u	interstitial flow velocity (m/day)
V_x	fracture pore volume (m^3)
w	mixing weight
z	specific power output function (kW/(m^3/day))
α	proportionality coefficient related to producer in the M-ARX method
β	proportionality coefficient related to injector in the M-ARX method
γ	constant governing the time lag of the response in the M-ARX method (days)
ϕ	porosity
ρ	density (kg/m^3)
τ	dimensionless time
θ	dimensionless ratio of heat capacities
ξ	dimensionless distance or pore volume

Subscripts

a	average
D	dimensionless variable
end	end of project life
f	fracture
$final$	final value in series of measurements
i	index, often associated with injector
I	injector or injection
j	index, often associated with producer
k	index, often associated with producer
m	matrix
P	producer or production
r	rock
w	water
O	initial value

to functions of time. The method works particularly well in fractured reservoirs because the fractures limit the variability in the streamlines between wells as the flow-rates change. The method relies on flow-rate and tracer data, which are used to determine the fracture pattern and characteristics roughly.

The objective of this work was to extend the characterization method of Juliusson (2012) such that it could be used to predict thermal drawdown and power output as a function of the flow-rate schedule. Moreover, an optimization problem for the flow rate schedule was formulated and solved. The goal was to maximize the NPV and the results were verified by comparison to results from numerical simulation.

2. Optimization model

As noted in Section 1, Lovekin and Horne (1989) carried out an early investigation into optimizing injection strategies for geothermal reservoirs. Macario (1991) and Sullera and Horne (2001) followed up on Lovekin's and Horne's method with applications to field data. Several reports by Shook (2001, 2003, 2004) also discuss the potential application of tracer data to infer reservoir properties that could, in turn, be used to optimize injection schedules. Other publications with reference to the topic take the approach of comparing a small number of preconceived options. For example, Barelli et al. (1995) investigated whether it would be better to produce at constant flow-rate or constant reservoir pressure from the Laderello geothermal field in Italy. More recently, Ganefianto et al. (2010) presented a paper on optimizing injection in the Salak geothermal field in Indonesia. Their work entailed a comparison of six injection scenarios, which were based on full-physics numerical reservoir simulations. Some of those scenarios also included alternative locations for reinjection. Juliusson et al. (2011) looked at the broader problem of optimizing how much energy should be extracted from a geothermal resource over time in order to achieve the most efficient utilization of the resource.

Methods for predicting thermal breakthrough in fractured reservoirs based on information from tracer tests have also been discussed, e.g., by Lauwerier (1955), Gringarten and Witherspoon (1975), Gringarten and Sauty (1975), Bodvarsson and Pruess (1984), Kocabas (2005), and Wu et al. (2008).

In our work, the objective function is designed to maximize the net present value of production revenue from the reservoir. The objective function thus depends on both economic parameters and physical models that are used to predict thermal decline and total energy output from the field. The objective function is defined as:

$$O(\boldsymbol{q_I}) = \sum_{j=1}^{N_P} \int_0^{t_{end}} P(t) z_j(T_{Pj}(t, \boldsymbol{q_I}), T_I, T_{P,\min}) q_{Pj}(\boldsymbol{q_I}) e^{-rt} dt \quad (1)$$

where $P(t)$ denotes the unit price of energy as a function of time, t, and r denotes the continuously compound interest rate for the investment. The number N_P indicates the number of production wells, the vector $\boldsymbol{q_I}$ refers to the injection rates for all of the injectors and q_{Pj} denotes the production rate for well j. The injection and production temperatures are given by T_I and T_P, respectively, and $T_{P,min}$ is the minimum design temperature for a given power plant utilizing the geothermal fluid.

An empirical correlation is used to compute the specific power output, z, as a function of the injection and production temperature. For this we use a modification of the correlation presented by Bennett and Horne (2011) and Tester et al. (2006). The specific power output from Bennett and Horne converted to units of kW/(m^3/day), is:

$$z_j'(T_{Pj}(t, \boldsymbol{q_I}), T_I) = 3.854 \times 10^{-15}(T_{Pj}(t, \boldsymbol{q_I}) - \zeta)^2 - 1.268 \times 10^{-3}(T_{Pj}(t, \boldsymbol{q_I}) - \zeta) - 2.123 \times 10^{-2} \quad (2)$$

with:

$$\zeta = 0.563 T_I - 14.51 \quad (3)$$

and temperature is in degree Celcius. Our modification is to include a minimum design temperature threshold ($T_{P,min}$) in the power output correlation. This threshold is modeled by a smooth function (*erf*) to avoid complications in the optimization procedure. Thus,

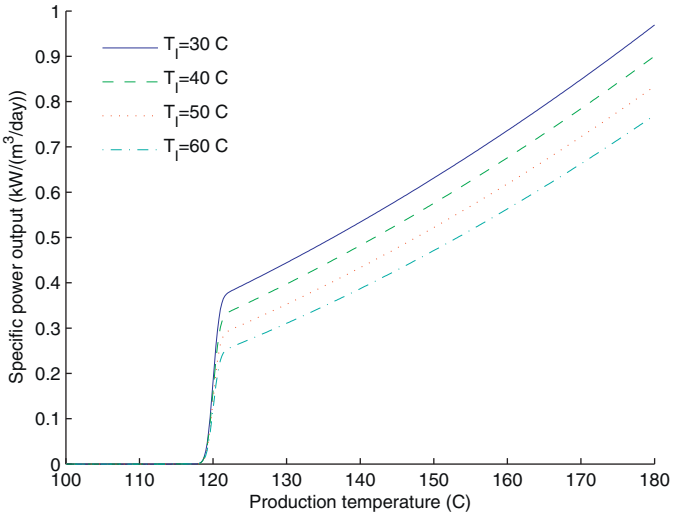

Fig. 1. Specific power output correlation as a function of injection and production temperature. A minimum design temperature threshold of 120 °C was applied in this case.

the specific power output from producer j is defined as:

$$z_j(T_{Pj}(t,\boldsymbol{q_I}),T_I,T_{P,\min})=\frac{1}{2}(erf(T_{Pj}(t,\boldsymbol{q_I})-T_{P,\min})+1)z'_j(T_{Pj}(t,\boldsymbol{q_I}),T_I) \tag{4}$$

where *erf* denotes the error function and $T_{P,min}$ denotes the minimum design temperature for the power plant. It is assumed that the injection temperature, T_I, is the same for all of the injection wells. The specific power output curve is plotted as a function of production and injection temperature, with a design threshold of 120 °C, in Fig. 1.

The time-dependent production temperature is computed as:

$$T_{Pj}(t,\boldsymbol{q_I})=\sum_{i=1}^{N_I}F_{ij}\frac{q_{Ii}}{q_{Pj}}T_{ij}(t,q_{Ii})=\sum_{i=1}^{N_I}F_{ij}\frac{q_{Ii}}{q_{Pj}}(T_0-(T_0-T_I)T_{D,i,j}(t,q_{Ii})) \tag{5}$$

The parameter F_{ij} represents the interwell connectivity (IWC) between injector i and producer j (Albertoni and Lake, 2002; Yousef et al., 2005; Dinh, 2009; Lee, 2010; Juliusson, 2012). The IWC parameters are particularly useful because they can be used to predict the production rates as a linear function of the injection rates, $\boldsymbol{q_P}=\boldsymbol{F^T q_I}$. The main limitation to the use of the IWC is that the reservoir should have low compressibility characteristics, i.e. it should be liquid-dominated.

In this work, the M-ARX method is used to infer the IWC based on flow-rate data (Lee, 2010). The governing equation for the M-ARX method is derived from a set of volume balances (accumulation = input–output from sources and sinks):

$$\frac{dq_{Pj}(t)}{dt}+\sum_{k=1}^{N_P}\frac{\alpha_{jk}}{\gamma_j}q_{Pk}(t)=\sum_{i=1}^{N_I}\frac{\beta_{ji}}{\gamma_j}q_{Ii}(t) \tag{6}$$

where α and β are proportionality coefficients and γ is a constant that governs the time lag of the response in the producers. The set of volume balances defined by Eq. (6) can be represented in discrete time as a matrix-vector equation:

$$\boldsymbol{q_P}(n+1)=-\boldsymbol{A}\boldsymbol{q_P}(n)+\boldsymbol{B}\boldsymbol{q_I}(n) \tag{7}$$

where n is a time-like discrete variable, and $\boldsymbol{A}$ and $\boldsymbol{B}$ are matrices containing the discrete counterparts of α_{jk}/γ_j and β_{ji}/γ_j, respectively. Eq. (7) defines a Multivariate AutoRegressive model for determining $\boldsymbol{q_P}$ with eXogenous inputs, $\boldsymbol{q_I}$ (hence the abbreviation M-ARX). A set of $n+1$ measurements yields n equations which can be solved together to find the elements of $\boldsymbol{A}$ and $\boldsymbol{B}$:

$$[\boldsymbol{q_P}(2)\dots\boldsymbol{q_P}(N+1)]=[-\boldsymbol{A}+\boldsymbol{B}]\begin{bmatrix}\boldsymbol{q_P}(1)&\dots&\boldsymbol{q_P}(N)\\ \boldsymbol{q_I}(1)&\dots&\boldsymbol{q_I}(N)\end{bmatrix} \tag{8}$$

The solution to Eq. (7) is stable, as long as $0\preceq(\boldsymbol{I}+\boldsymbol{A})^{-1}\boldsymbol{B}\preceq 1$ (elementwise). It can be shown via the Z-transform (discrete analog of Laplace transform) that if the injection rates are kept constant, the production rates will stabilize at:

$$\boldsymbol{q_P}=(\boldsymbol{I}+\boldsymbol{A})^{-1}\boldsymbol{B}\boldsymbol{q_I}=\boldsymbol{F}\boldsymbol{q_I} \tag{9}$$

The elements of the matrix $\boldsymbol{F}=(\boldsymbol{I}+\boldsymbol{A})^{-1}\boldsymbol{B}$ then define the interwell connectivity for each of the injector–producer pairs in terms of flow-rate. Thus, the portion of flow leaving injector i arriving at producer j will be $q_{IiPj}=F_{IiPj}q_{Ii}$.

The temperature T_0 in Eq. (5) refers to the initial temperature in the reservoir and $T_{D,i,j}$ represents a function of dimensionless temperature as reported by many authors that have discussed thermal breakthrough in fractured reservoirs. For example, using Lauwerier's (1955) formulation:

$$T_{D,ij}(t,q_{Ii})=erfc\left(\frac{\xi_{ij}}{2\sqrt{\theta(\tau_{ij}-\xi_{ij})}}\right)U(\tau_{ij}-\xi_{ij}) \tag{10}$$

In this formula *erfc* denotes the complementary error function and U is the unit step function. The dimensionless variables ξ, τ and θ are defined as:

$$\xi_{ij}=\frac{K_r}{b_{ij}^2\rho_w C_w}\frac{V_{x,ij}}{R\phi_f F_{ij}q_{Ii}} \tag{11}$$

$$\tau_{ij}=\frac{K_r}{b_{ij}^2\rho_{af}C_{af}}t \tag{12}$$

$$\theta=\frac{\rho_{af}C_{af}}{\rho_{am}C_{am}} \tag{13}$$

where b_{ij} denotes the fracture half-aperture, ϕ_f is the fracture porosity, K_r is the thermal conductivity of the rock, $R=1+\phi_m(1-\phi_f)/\phi_f$ is the tracer retardation factor with ϕ_m representing the matrix porosity. The groups:

$$\rho_{af}C_{af}=\phi_f\rho_w C_w+(1-\phi_f)\rho_r C_r \tag{14}$$

and

$$\rho_{am}C_{am}=\phi_m\rho_m C_m+(1-\phi_m)\rho_r C_r \tag{15}$$

represent the average volumetric heat capacity for the fracture and the surrounding rock matrix, respectively.

The thermodynamic parameters needed in Eq. (10) can be estimated based on existing knowledge of the petrology and reservoir fluid. The largest uncertainties are usually related to the geometry of the flow paths. The pore volume can be estimated by the first moment of a slug tracer return curve:

$$V_{x,ij}=\frac{\int_0^{Q_{ij}(t_{final})}Q'_{ij}c_{ij}^{impulse}(Q'_{ij})\,dQ'_{ij}}{\int_0^{Q_{ij}(t_{final})}c_{ij}^{impulse}(Q'_{ij})\,dQ'_{ij}} \tag{16}$$

where $Q_{ij}(t)=\int_0^t F_{ij}q_{Ii}(\tau)\,d\tau$ denotes the cumulative flow between wells and $c_{ij}^{impulse}(Q_{ij})$ is the tracer concentration from a slug tracer test, as a function of cumulative well-to-well flow. A benefit of using (16) to compute the pore volume is that it is applicable for tracer data collected under variable flow rate conditions. Theoretically, t_{final} should tend to infinity, but in practice it could be taken as the last measurement time, or some time value where the tail of the tracer return has become very small. A formulation similar to Eq. (16) can be used to find V_x using tracer kernels (Juliusson, 2012).

Methods to determine ϕ_f, b, or the group $\phi_f b$, which appears upon simplification of Eq. (10), have not been well established. Thermally reactive tracer methods like those proposed by Reimus et al. (2011) seem promising, but are still in development. It should also be noted that the Lauwerier (1955) solution assumes flow through a single fracture surrounded by a matrix of infinite extent. Thus, this solution will tend to give optimistic results, especially at late times when thermal interaction between parallel flow paths may have become significant.

With the aforementioned definitions, the optimization problem for injection rate scheduling can be presented as:

$$\max_{q_I} \quad O(\boldsymbol{q_I}) = \sum_{j=1}^{N_p} \int_0^{t_{end}} P(t) z_j(T_{Pj}(t, \boldsymbol{q_I}), T_I, T_{P,\min}) q_{Pj}(\boldsymbol{q_I}) e^{-rt}\, dt \tag{17}$$

$$\text{subject to} \quad \sum_{i=1}^{N_I} q_{Ii} \le q_{I,tot} \tag{18}$$

$$q_{Ii} \le q_{Ii,\max}, \quad i = 1, \ldots, N_I \tag{19}$$

$$q_{Ii} \ge 0, \quad i = 1, \ldots, N_I \tag{20}$$

In other words, the goal is to find the set of injection rates, $\boldsymbol{q_I}$, that maximizes the objective function, O, subject to constraints on the total injection rate, $q_{I,tot}$, and $q_{Ii,max}$ and individual well injection rates.

Two examples that illustrate the application of this optimization method are given in the following sections. In each of the examples, the initial temperature is assumed to be 150 °C and the injection temperature is 50 °C. As an initial guess, the flow-rates are assumed to be distributed evenly between the injectors, with a reasonable maximum rate, $q_{Ii,max}$. The producers are set to a constant bottomhole pressure. The porosity and thermodynamic properties of rock and water are assumed to be known. The unknown variables that need to be determined from production data are the IWCs, F, the fracture pore volumes, V_x, and the fracture half-apertures, b.

The optimization problem was solved with MATLAB's built-in optimization function fmincon (MathWorks, 2012), which is designed to solve constrained nonlinear optimization problems. The interior-point algorithm was used to solve the problems presented here. The solution times were minimal, on the order of a few seconds. Nothing conclusive will be stated about the regions of convexity for the problem (Boyd and Vandenberghe, 2004). However, based on contour plots of the objective function for the cases investigated, the objective function seems to be nonconvex in general (had multiple local maxima), but convex in the area of interest. As a result, the optimization problem is easy to solve computationally.

3. Example I: small scale reservoir model

A discrete fracture model (Reservoir Model I) was created as a test case for the first injection rate optimization example. This example was made especially simple to illustrate the method. The model, shown in Fig. 2, was built using the groundwater simulation software FEFLOW (DHI-WASY, 2010) and the computational gridding software Triangle (Shewchuk, 1996). The main properties of Reservoir Model I are summarized in Table 1. The model has two injectors and two producers and the aim is to determine those injection rates that maximize the net present value of production over a 30 year period.

Synthetic flow-rate and tracer data were generated to infer the well-to-well characteristics. The flow-rate data are shown in Fig. 3 and the tracer concentration data are shown in Fig. 4.

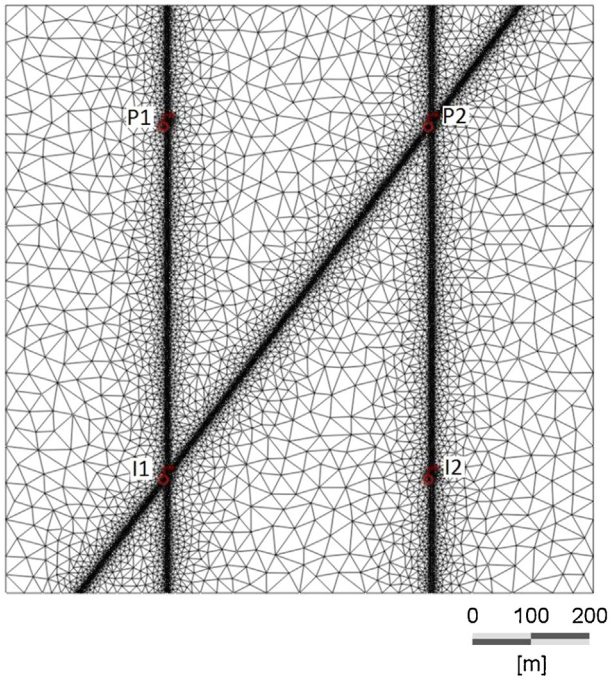

Fig. 2. Computational grid for Reservoir Model I.

Table 1
Properties for Reservoir Model I.

General	
Dimensions	1000 m × 1000 m × 500 m
Longitudinal dispersivity	50 m
Transverse dispersivity	5 m
Rock heat capacity	2520 kJ/m^3/C
Rock heat conductivity	3 J/m/s/C
Fractures	
Number of fractures	3
Discrete fractures	Yes
Porosity	0.05
Hydraulic conductivity	0.01 m/s
Total compressibility	10^{-10} Pa^{-1}
Matrix	
Porosity	0.001
Hydraulic conductivity	2×10^{-9} m/s
Total compressibility	10^{-11} Pa^{-1}

The IWCs, listed in Table 2, were obtained by applying the M-ARX method (Lee et al., 2010) to the flow-rate data. The pore volumes, listed in Table 3, were estimated by applying Eq. (16)

Table 2
Interwell connectivity for Reservoir Model I.

F	P1	P2
I1	0.5477	0.4486
I2	0.0024	0.9871

Table 3
Fracture pore volume for Reservoir Model I, as estimated from slug tracer tests. The true pore volume (as specified in the FEFLOW model) for the I1–P1 and I2–P2 connections was 15,000 (m^3), and for the I1–P2 connection it was 18,750 (m^3).

V_x (m^3)	P1	P2
I1	13,492	17,238
I2	∞	14,505

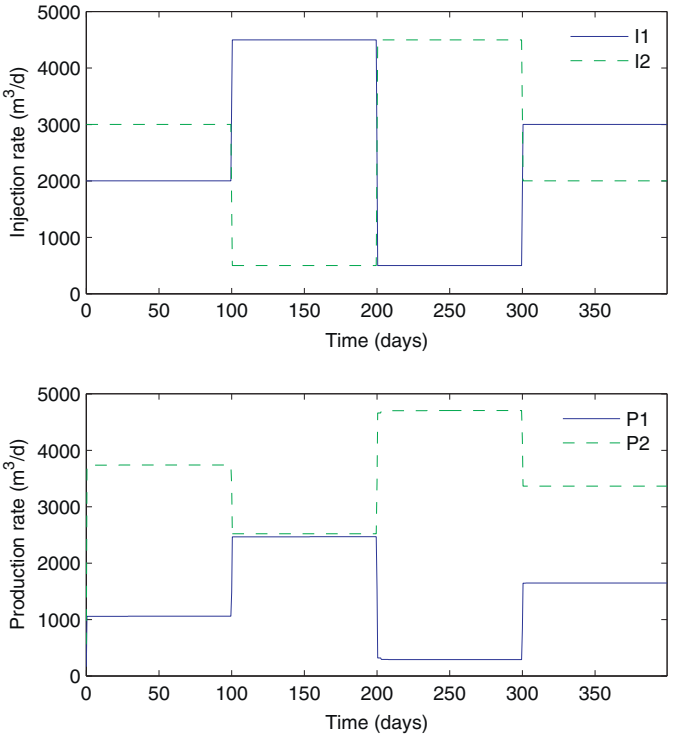

Fig. 3. Flow-rate history for Example I.

to the tracer data shown in Fig. 4. The pore volume for the I2–P1 connection was assumed to be infinite because no tracer broke through.

The IWCs and pore volumes were used to calibrate the objective function. It was also assumed that the effective half-aperture, $b\phi_f = 0.025$ m, was known. As stated earlier, the effective aperture would be hard to quantify in practice, but it was assumed to be known to illustrate the applicability of the optimization method.

3.1. Optimization of injection rates

In the case illustrated here, the injection rates were constrained to be below 4000 m^3/day for well I1 and 3000 m^3/day for well I2. The total injection rate was constrained to be less than or equal to 5000 m^3/day. As an initial guess, it was assumed that 2500 m^3/day were being injected into each well. In the NPV calculation, the interest rate was $r = 8\%$ and the present value of energy price, $P(t)$, increased over a 30 year period, from 60 to 120$/MWh with an added 2% inflation.

Solving the problem yielded an optimal allocation rate of 1652 m^3/day (64%) for I1 and 844 m^3/day (36%) for I2. The objective function and constraints are shown in Fig. 5.

The success of the optimization method depended on how well the thermal breakthrough could be predicted by the analytical heat transfer equations. To investigate this, the thermal drawdown, $T_{Pj}(t,\boldsymbol{q_I})$, predicted by Eq. (5), was compared to the simulated values. Comparisons were made with equal injection into each injector (Fig. 6) and at the optimal injection configuration (Fig. 7). As the figures show, the Lauwerier solution provided a relatively accurate estimate of the thermal breakthrough curve.

The optimal solution in this case was well below the maximum allowable injection rate. This was because the power output would drop significantly if the production temperature fell below 120 °C. Fig. 7 shows how the predicted temperature converged to a value close to 120 °C near the end of the production period for producer P2. The temperature in producer P1, however, was allowed to fall below the 120 °C threshold at an earlier time. This shows that the

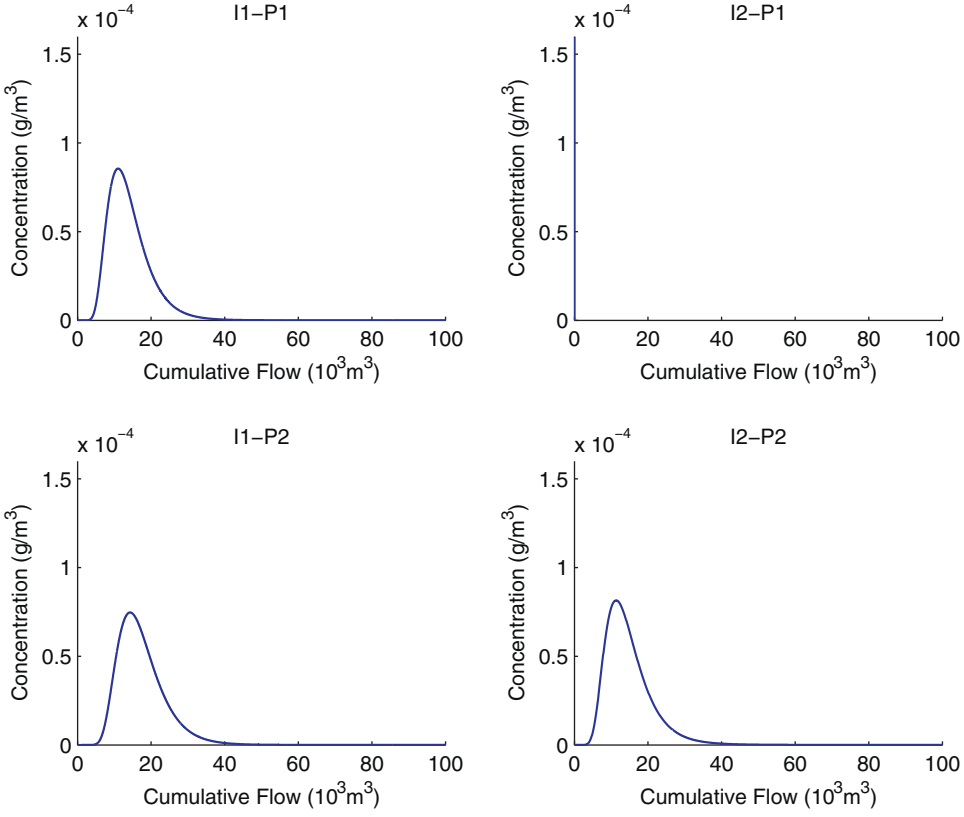

Fig. 4. Slug tracer returns shown as a function of cumulative injector-to-producer flow in Reservoir Model I.

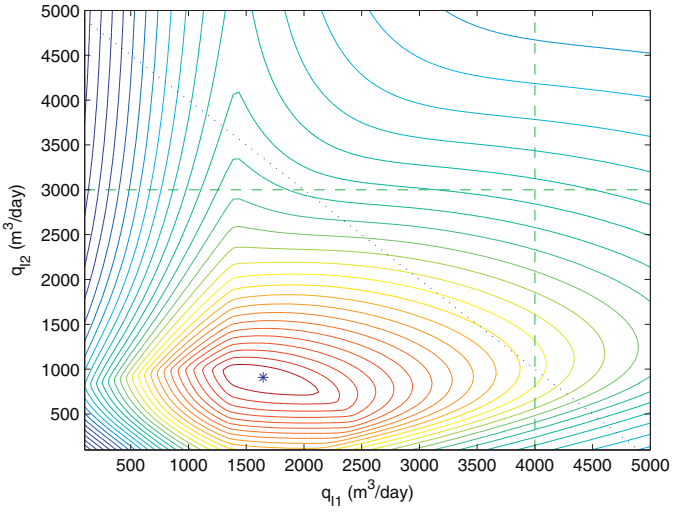

Fig. 5. A contour plot of the objective function. A maximum total injection constraint of 5000 m^3/day is illustrated by the blue diagonal line. Maximum injection constraints of 4000 and 3000 m^3/day for injectors I1 and I2, respectively, are shown by the green dashed lines. The optimum feasible point is given by the blue star. (For interpretation of the references to color in this figure legend, the reader is referred to the web version of the article.)

relative benefit of keeping P2 at a high production rate at the late stages outweighed the benefit of maintaining production in P1 at late stages. Comparison to the simulated thermal returns shows that the actual decline in production would occur somewhat earlier than predicted by the analytical model.

The increase in the objective function over the initial guess (where all injection rates were equal) was quite significant, about 91%. This number can be deceiving though because it is given relative to an arbitrary initial guess for the flow rates. The number does not, however, include the savings that would be made by building a smaller power plant, if one knew from the beginning that a smaller total flow rate would actually yield higher returns over the 30 year period. Taking the plant size into consideration in the objective should lead to even smaller optimal flow rates.

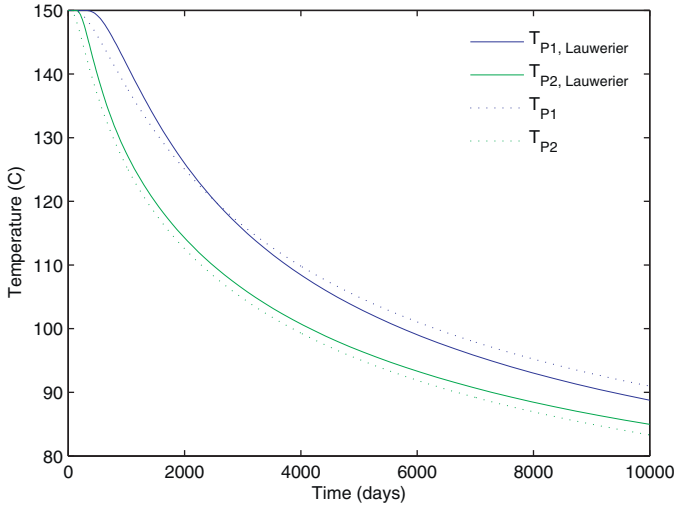

Fig. 6. Comparison of simulated thermal breakthrough (dotted curves) and thermal breakthrough as predicted by the Lauwerier (1955) analytical model (solid curves). For this case water at 50 °C was injected at 2500 m^3/day into each of the two injectors.

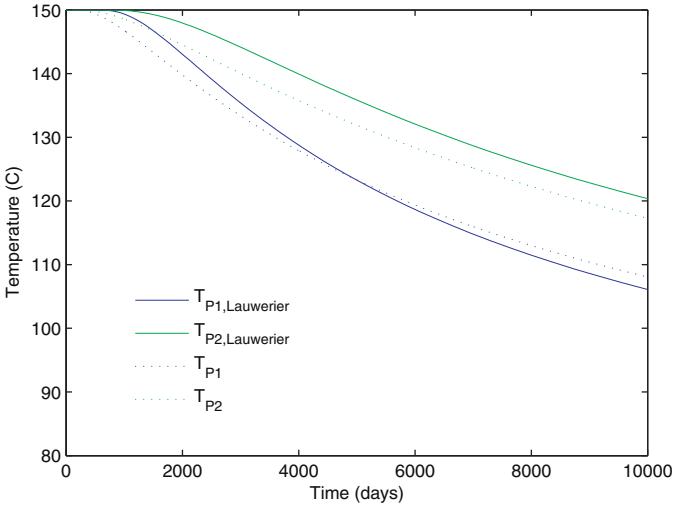

Fig. 7. Simulated thermal breakthrough (dotted curves) and thermal breakthrough as predicted by the Lauwerier (1955) analytical model (solid curves). For this case water at 50 °C was injected at the optimal allocation of 1652 m^3/day into injector I1 and 844 m^3/day into I2.

4. Example II: larger scale reservoir model

The reservoir model used for the second example (Reservoir Model II) was based partially on the structure of the fractured Soultz-sous-Forêts enhanced geothermal system in France (Genter et al., 2010). A three-dimensional map of the main fractures was obtained from Place et al. (2011). The fractures were imported into the discrete fracture generation software FRACMAN. Additional fractures were generated based on data from Massart et al. (2010), and then a two-dimensional horizontal slice, 3000 m × 1000 m, of fracture traces was extracted from a region of interest. Reservoir Model II had four injection wells and three production wells. The computational grid for the two-dimensional slice is shown in Fig. 8 and the main properties of the FEFLOW reservoir model are given in Table 4. A more detailed description of the construction of Reservoir Model II is given in Juliusson (2012).

It was assumed that some porosity estimates and wellbore imaging data were available (as is the case for the Soultz reservoir) such that an educated guess might be made about the average effective fracture aperture. Any additional reservoir information from the underlying model was ignored. The intent was to test how well the optimization method would perform based on data that could be measured in the field, using conventional measurement methods.

Table 4
Summary of properties for Reservoir Model II.

General	
Dimensions	3000 m × 1000 m × 500 m
Longitudinal dispersivity	50 m
Transverse dispersivity	5 m
Rock heat capacity	2520 kJ/m^3/C
Rock heat conductivity	3 J/m/s/C
Fractures	
Number of fractures	19
Discrete fractures	Yes
Porosity	0.03
Hydraulic conductivity	$\propto L^{1.87}$ m/s
Total compressibility	10^{-10} Pa^{-1}
Matrix	
Porosity	0.001
Hydraulic conductivity	10^{-10} m/s
Total compressibility	10^{-11} Pa^{-1}

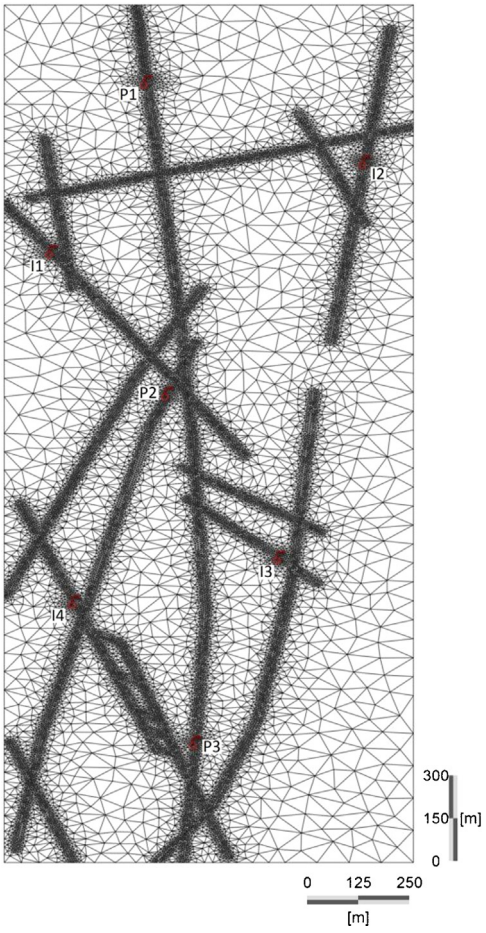

Fig. 8. Computational grid for Reservoir Model II. Wells I1, P2 and I3 represent wells GPK2, GPK3 and GPK4, respectively, in the actual Soultz reservoir.

4.1. Tracer returns at various flow rate configurations

Reservoir Model II was used to investigate the variability in tracer returns under various injection rate configurations. Table 5 lists the simulation runs, which involved seven different injection rate configurations. Tracer was injected with a constant continuous concentration into each of the injectors, one at a time, and the produced concentration was recorded over a period of 300 days. Tracer was injected continuously as opposed to a slug injection because of computational challenges with the latter method. A total of 28 simulations were run.

Fig. 9 shows the distribution of tracer in the reservoir when 3000 m^3/day had been injected into each injector over a period of 300 days (i.e. runs 25–28).

Table 5
List of various injection rate configurations used. Four simulations were run for each flow rate configuration, where tracer was allocated to one injection well for each simulation. A total of 28 simulations were run.

Flow rate config. #	I1 (m^3/day)	I2 (m^3/day)	I3 (m^3/day)	I4 (m^3/day)
1	1200	1200	4800	4800
2	1200	4800	1200	4800
3	1200	4800	4800	1200
4	4800	1200	1200	4800
5	4800	4800	1200	1200
6	4800	1200	4800	1200
7	3000	3000	3000	3000

There were 12 injector–producer connections. The tracer returns for each connection, at each of the seven flow configurations, are shown in Fig. 11. It was clear from these results that the tracer returns varied significantly as a function of the injection rate configuration. The variation was seen in terms of the mean arrival time, the tracer dispersion, and the fraction of the initial concentration recovered.

The IWC was computed based on flow-rate data using the M-ARX method. The step-wise varying flow-rates, shown in Fig. 10, were used to compute these parameters.

The IWC could also be computed based on the stabilized tracer concentration at each producer. This was done by equating the stabilized tracer concentration to the fraction of injection water arriving at the producer, i.e.:

$$\frac{c_{ij}^{continuous}(t_{final})}{c_{Ii}^{continuous}} = \tilde{F}_{ij}\frac{q_{Ii}}{q_{Pj}} \tag{21}$$

Thus, the tracer-based IWC is:

$$\tilde{F}_{ij} = \frac{c_{ij}^{continuous}(t_{final})}{c_{Ii}^{continuous}}\frac{q_{Pj}}{q_{Ii}} \tag{22}$$

The tracer-based IWC, $\tilde{F}_{ij}$, is the equivalent of F_{ij} in Eq. (5). The only difference is that $\tilde{F}_{ij}$ is computed from tracer data, whereas F_{ij} is based on flow-rate data.

The flow-rate-based and tracer-based IWCs are compared in Fig. 12. This comparison shows that the tracer-based IWCs are generally more extreme than the flow-rate-based IWCs. In other words, the tracer based IWC values are generally closer to 0 or 1, than the flow-rate-based IWCs which are generally closer to the average of $1/N_p$. This is likely because the flow-rates are governed by the pressure (or diffusion) equation, which has a smoothing effect, while the tracer travels in a more advective manner, i.e. along the main flow paths. A relatively large variability in the tracer-based IWC as a function of the injection rate configuration was also observed (Fig. 12). This variability was partially attributable to insufficient simulation time and numerical inaccuracy in the simulations; in addition, some variability was caused by changes in the flow paths taken between each injector–producer pair.

The continuous tracer returns needed to be converted to the equivalent impulse return curves, such that the fracture pore volumes could be estimated from Eq. (16). This was accomplished with:

$$c_{ij}^{impulse}(Q_{ij}) = \frac{1}{c_{ij}^{continuous}(t_{final})}\frac{\partial c_{ij}^{continuous}(Q_{ij})}{\partial Q_{ij}}, \tag{23}$$

assuming unit mass production. These unit mass responses are essentially the tracer kernels (Juliusson, 2012). Note that the way the cumulative flow, Q_{ij}, is computed depends on the IWC. Therefore, the pore volume estimates depend on whether the tracer-based or flow-rate-based IWC is used. Fig. 13 shows the unit impulse responses (tracer kernels) computed from each of the different configurations. The location of the peak of each impulse response is a rough indicator of the estimated pore volume – the actual pore volume is measured by the first moment, which is slightly larger.

The pore volume estimates for the average response and the response with flow rate configuration 7 are shown in Tables 6 and 7, respectively. Note that when there was poor connectivity between the wells, the tracer traveled very slowly along the corresponding connection. Thus, very little tracer had been delivered along the connection over the 300 day testing period, resulting in a truncated tracer return curve. This led to an underestimate in the pore volume, as it was computed from a numerical integration of the tracer return data. A color coding is used in the tables to indicate

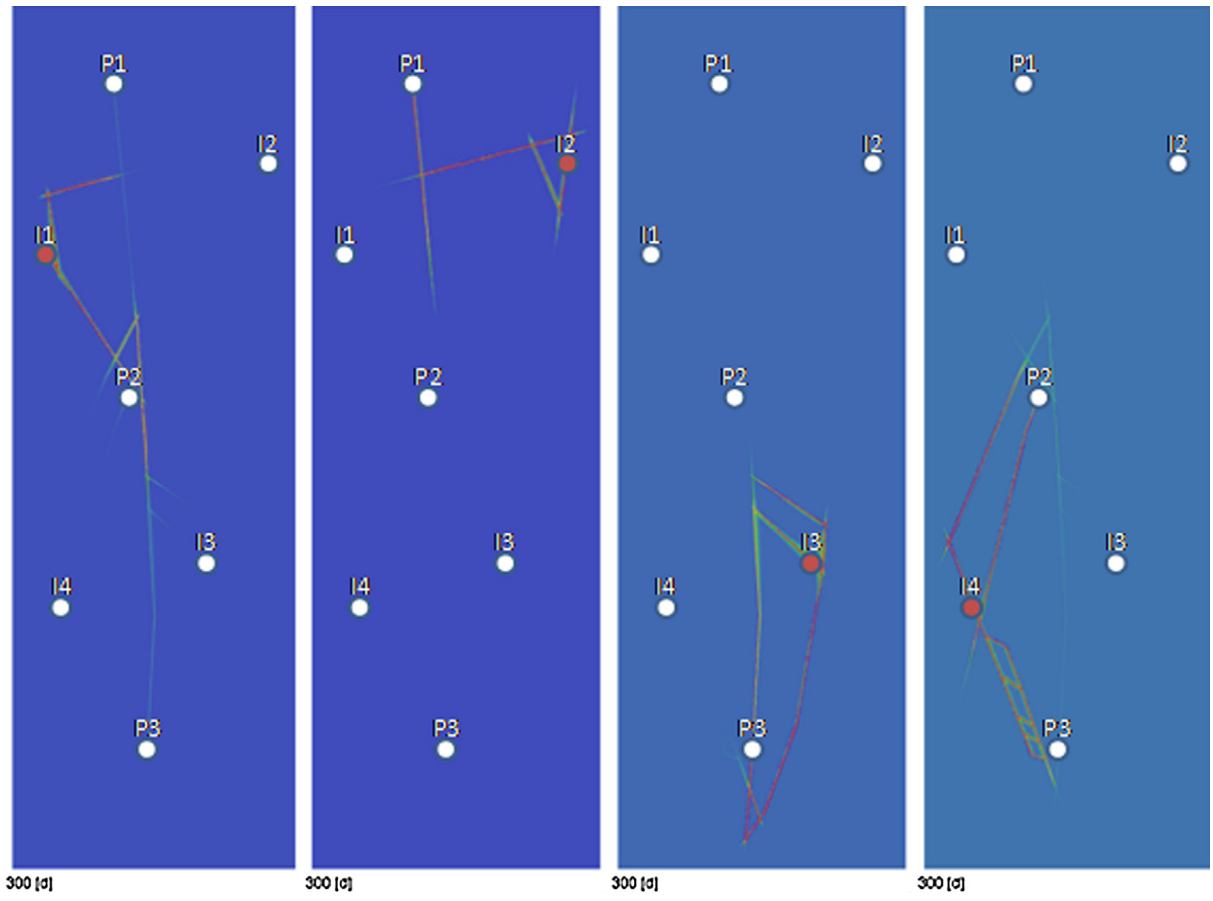

Fig. 9. The tracer distribution in the reservoir after 300 days of tracer injection, into wells I1 through I4, going from left to right. The injection rate was 3000 m^3/day for each injector (i.e. flow rate configuration 7).

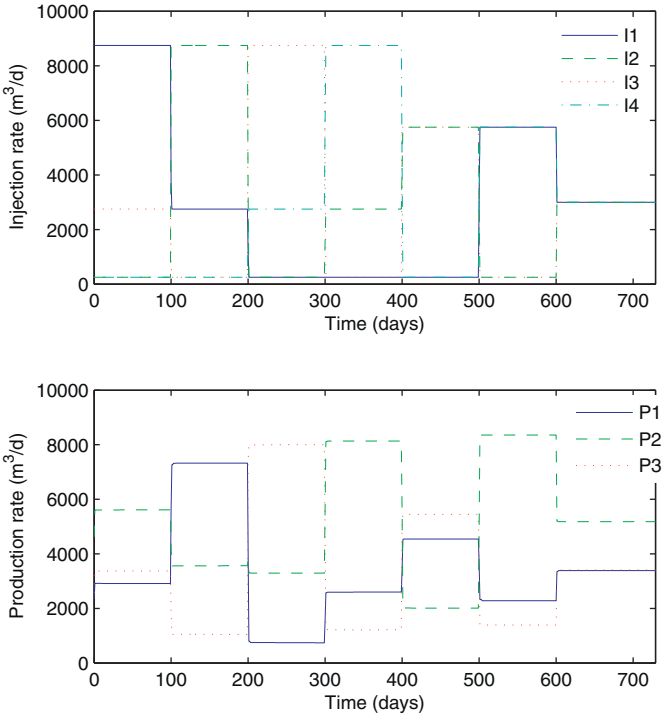

Fig. 10. Flow-rate data used to compute the IWC for Example II.

loosely how much tracer return data was available (i.e. how much of the tail seemed to be truncated). The problem of missing tails was accounted for, partially, by averaging the responses, which is why more reasonable estimates were found using the averaging method than just the tracer returns from flow rate configuration 7. Nevertheless, it was obvious, for example, that there was a fracture connection of large volume between I3 and P1 (observe Fig. 8). Erroneous estimates of this kind needed to be corrected. In practice, one might guess that if a very small fraction of tracer was returned, that probably meant that there was a very large pore volume separating the two wells or that there was a very small flow-rate running between the wells in question. A small flow-rate should correspond to a small flow-rate-based IWC, *F*.

Table 6
Estimated pore volume of each injector–producer connection, as computed from the average response of all simulated injection rate configurations. The color coding refers to the presumed quality of the estimates; red is poor, yellow is medium and green is good. Volume estimates are in m^3.

V_x [m^3]	*P1*	*P2*	*P3*
I1	19,052	22,018	18,864
I2	28,920	17,719	11,796
I3	405	16,413	71,227
I4	7,972	34,272	16,432

Table 7
Estimated pore volume of each injector–producer connection, as computed from the response with all injection rates equal (config. 7). The color coding refers to the presumed quality of the estimates; red is poor, yellow is medium and green is good. Volume estimates are in m^3.

V_x [m^3]	*P1*	*P2*	*P3*
I1	8,367	24,903	241
I2	32,691	1,848	1
I3	0	17	65,371
I4	1	41,235	14,676

Table 8
Interwell connectivity (IWC) parameters used for optimization. These are the average values of those parameters estimated by flow-rate variations and tracer returns.

F	P1	P2	P3
I1	0.201	0.692	0.056
I2	0.876	0.103	0.030
I3	0.022	0.052	0.971
I4	0.031	0.869	0.080

4.2. Optimization of injection rates

An injection strategy was designed for Reservoir Model II, based on simulated flow-rate and tracer data. It was assumed that flow-rate-based IWCs were available, along with tracer returns obtained with all injection rates equal to 3000 m^3/day (config. 7, Table 5). It was also assumed that some core samples were available, along with wellbore imaging logs that would give an idea about the aperture and porosity of the larger fractures in the reservoir. Any additional knowledge about the reservoir was ignored.

The average of the flow-rate and tracer-based IWC, shown in Table 8, was used to compute the injector–producer flow-rates and cumulative flow.

The direct estimation of the pore volumes using these IWCs yielded the results shown in Table 9.

The inadequate pore volume estimates corresponded to cases where relatively little tracer had been recovered. As explained earlier, this did not necessarily mean that there was no fracture connection between the wells in question. It could have been that the measurement time was not long enough, because the interwell flow-rate was small, as indicated by the IWC estimates. Thus, we used the good connections to compute an average pore volume over the aerial distance between wells. This yielded $V_x/L \approx 48$ m^2, which lead to the estimated pore volumes shown in Table 10. Another possibility would have been to assume that each of the inadequate connections had an infinite pore volume, as was done in Example I, or to use a parametric tracer return model estimate V_x.

The ratio of the pore volume to the IWC could be used as an indicator of the time until thermal breakthrough (Table 11). This can be seen by writing out Lauwerier's (1955) solution in the form

Table 9
Estimated pore volume using IWC parameters from Table 8 and tracer returns from flow rate configuration 7. Inadequate estimates are labeled in yellow.

V_x [m^3]	*P1*	*P2*	*P3*
I1	17,116	21,419	10,423
I2	27,807	75,070	24,325
I3	8,263	17,086	59,393
I4	5,776	39,768	18,229

Table 10
Estimated pore volumes used for optimization.

V_x [m^3]	*P1*	*P2*	*P3*
I1	17,116	21,419	82,304
I2	27,807	43,908	97,164
I3	79,572	29,001	59,393
I4	85,899	39,768	18,229

Table 11
Ratio of pore volume to IWC estimated for the optimization problem. Smaller values indicate more interaction (four of the best connections are shown in bold font).

V_x/F [m^3]	P1	P2	P3
I1	85,015	**30,949**	1,464,266
I2	**31,733**	428,119	3,230,772
I3	3,595,986	561,737	**61,180**
I4	2,735,735	**45,775**	227,084

$$T_{D,i,j}(t, q_{Ii}) \approx erfc\left(\frac{\xi_{ij}}{2\sqrt{\theta\tau_{ij}}}\right) = erfc\left(\frac{V_{x,ij}}{F_{ij}q_{Ii}R\phi_f 2b_{ij}}\sqrt{\frac{K_r\rho_{am}c_{am}}{(\rho_w c_w)^2 t}}\right) \quad (24)$$

The pore volume to IWC ratio indicated that the largest interaction would be between well pairs P1–I2, P2–I1, P2–I4, and P3–I3.

Eq. (24) shows that the principal remaining uncertainty is with the group $R\phi_f b_{ij}$. In practice, some average estimate for the fracture and matrix porosity might be obtainable from core sampling, but determining the effective aperture would be challenging. For lack of a better method, the fracture half-aperture was taken as b_{ij}=1 m, i.e. an arbitrary value that was on the right order of magnitude (b_{ij} ranged from 0.2 to 1.5 in the actual model). Assuming that core data had given ϕ_m = 0.001 and ϕ_f = 0.03, then all the parameters required for Eq. (24) were available.

The optimization was performed using the IWCs and pore volumes given in Tables 8 and 10, respectively. An upper bound constraint of 4500 m^3/day was placed on the individual injection rates, and a 12,000 m^3/day constraint was placed on the total injection rate. As before, the interest rate was r = 8% and the energy price was increasing over a 30 year period in real terms, from 60 to 120$/MWh with an added 2% inflation. The optimal injection rates, based on these assumptions, are shown in Table 12.

The objective function could not be plotted in this case, as it is four-dimensional. However, slices of the objective function could be viewed, with two of the decision variables fixed at the optimal values. Fig. 14 shows a q_1–q_{I2} slice of the objective function with q_{I3} and q_{I4} fixed at the optimal values. These plots were useful to verify that the optimization algorithm had not become trapped in some local maximum.

Based on the analytical temperature estimates, the value of the objective function increased by 37% compared to the initial allocation of 3000 m^3/day per well. However, it is more meaningful to look at the improvement based on the simulations, because they were meant to represent the actual outcome of the injection

Table 12
Optimal injection rates for Example II.

q_{Ii}	m^3/day	%
I1	1225	20
I2	1244	20
I3	2145	35
I4	1516	25
$\sum Ii$	6130	100

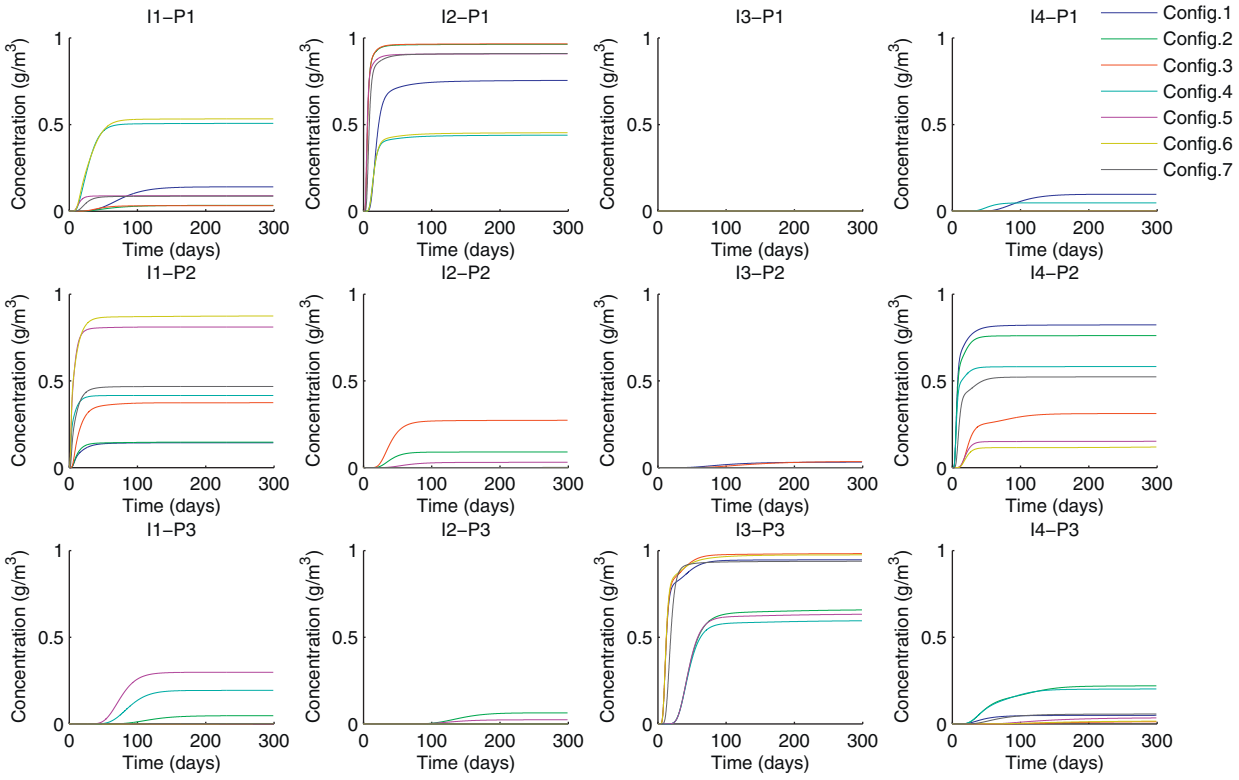

Fig. 11. An illustration of the tracer returns coming from each injector to each producer under various injection rate configurations.

strategy. The simulation based NPV for the initial allocation was \$19.7 million, while the optimized allocation yielded \$25.2 million. Thus, a 27% increase was obtained over the initial allocation.

The predicted and simulated thermal breakthrough curves are shown in Fig. 15 for the case when the flow was distributed evenly at 3000 m^3/day to each injector. The same curves for the optimal injection rates are shown in Fig. 16.

The predicted and simulated breakthrough curves matched surprisingly well, especially for the even injection case. This good match was a bit fortuitous because the aperture value was chosen somewhat arbitrarily. Better ways to characterize the fracture aperture are needed but hard to find.

An alternative to finding the fracture aperture would be to estimate the effective heat transfer area of the flow path. For example,

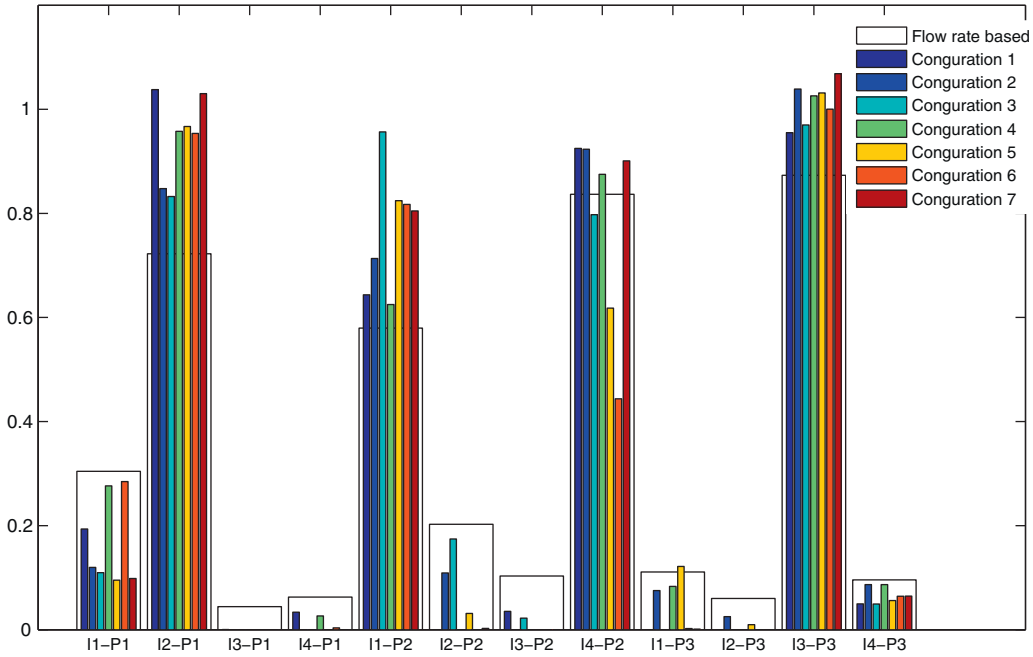

Fig. 12. A comparison of the flow-rate-based IWC and the tracer-based IWC computed at various flow rate configurations. Colored bars represent the tracer based IWC. (For interpretation of the references to color in this figure legend, the reader is referred to the web version of the article.)

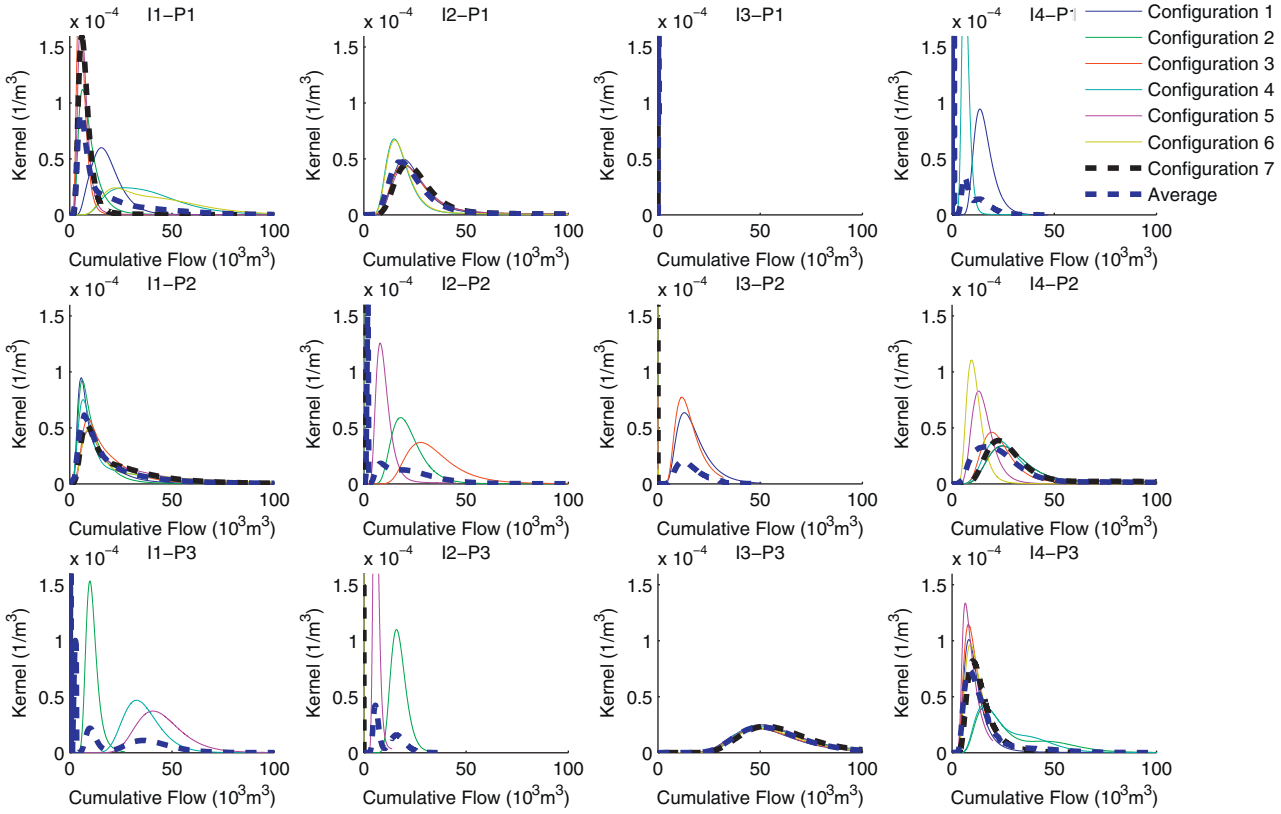

Fig. 13. Unit impulse tracer returns or tracer kernels for the various injection configurations listed in Table 5.

Eq. (24) can be written in terms of the effective heat transfer area, $A_{x,i,j}$, as follows:

$$T_{D,i,j}(t, q_{Ii}) \approx erfc\left(\frac{A_{x,i,j}}{F_{ij}q_{Ii}}\sqrt{\frac{K_r\rho_{am}c_{am}}{(\rho_w c_w)^2 t}}\right) \quad (25)$$

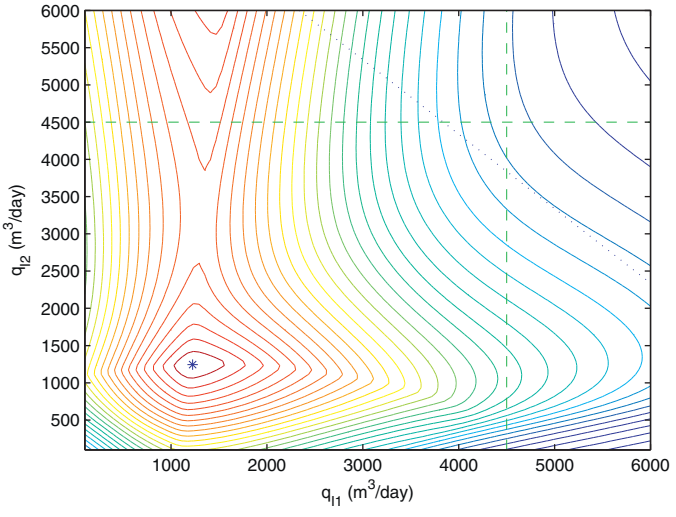

Fig. 14. A contour plot of a slice through the objective function based on net present value of production. The slice is taken with $q_{I3} = 2145\,m^3/day$ and $q_{I4} = 1516\,m^3/day$, which are the optimum values. A maximum total injection constraint of 12,000 m^3/day is illustrated by the blue diagonal line. Maximum injection constraints of 4500 m^3/day for injectors *I*1 and *I*2 are shown by the green dashed lines. The optimum feasible point is shown by the blue star. (For interpretation of the references to color in this figure legend, the reader is referred to the web version of the article.)

This way one could avoid having to determine the fracture volume and aperture and focus on ways to determine the size of the fracture surface, e.g., based on seismic imaging or reactive tracers.

5. Discussion

Two other objective functions were tested in the development of this work. The first was geared toward minimizing the total

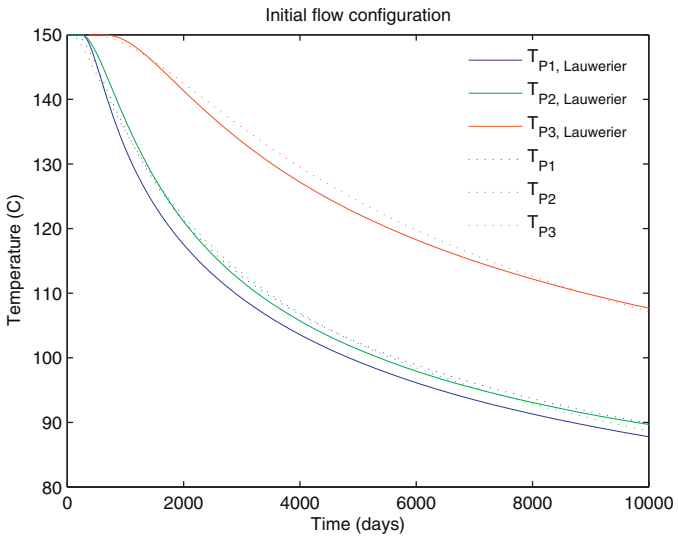

Fig. 15. Comparison of simulated thermal breakthrough (dotted curves) and thermal breakthrough as predicted by the Lauwerier (1955) analytical model (solid curves). For this case water at 50 °C was injected at 3000 m^3/day into each of the four injectors.

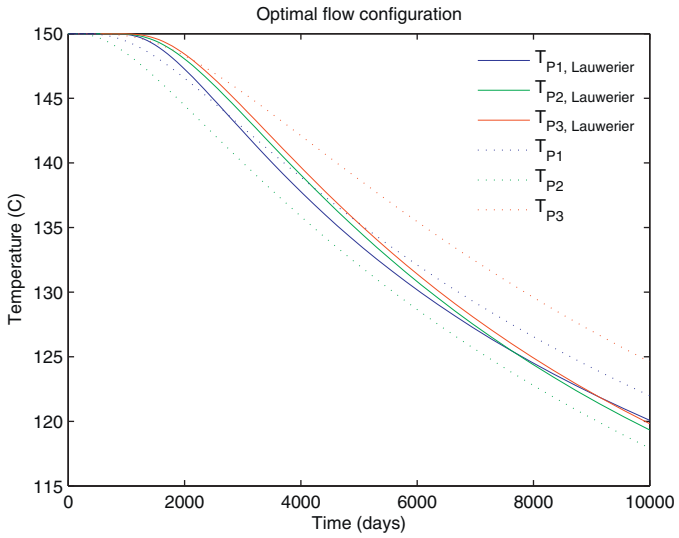

Fig. 16. Comparison of simulated thermal breakthrough (dotted curves) and thermal breakthrough as predicted by the Lauwerier (1955) analytical model (solid curves). For this case water at 50 °C was injected at the optimal flow-rates given in Table 12.

mass produced from a tracer test and hence did not require a thermal transport model. The second was focused on maximizing the amount of energy extracted from the reservoir over the project life. A drawback of using these models was that they would always suggest that the maximum allowable total injection rate should be used. For further discussion please refer to Appendix B of Juliusson (2012).

Preliminary tests with an upscaled three-dimensional fractured reservoir are reported in Juliusson (2012). The results showed that the Lauwerier (1955) thermal drawdown model is not well suited for characterizing such reservoirs. More research into analytical or semi-analytical ways to model thermal transport through three-dimensional fractured reservoirs would be useful.

A topic of interest related to better thermal transport modeling would be the application of thermally degrading tracers to determine the effective aperture or heat transfer area. Reimus et al. (2011) have made progress on that front but their work is still in development.

Injection and production scheduling models have been studied quite thoroughly for oil and gas reservoirs. A few publications of interest are those by Sarma et al. (2006), Cardoso et al. (2009), Echeverria Ciaurri et al. (2011) and Jansen (2011). Much of this work has been focused on closed-loop optimization problems. In these problems, an objective function based on the NPV of production is usually defined. Then the optimization problem is constrained by the arbitrarily complex discretized differential equations which represent the mass and energy balances that form the basis of a full-physics reservoir simulator.

6. Conclusions

An optimization approach has been suggested based on maximizing the net present value (NPV) of production revenue from the reservoir. An empirical correlation has been used to relate the injection and production temperature to the specific electrical power output. The power output model, in conjunction with predictions for the future energy prices and interest rates, allows the computation of the NPV as a function of the injection rates. The theory and example applications presented here have shown that the flow rate scheduling problem, for fractured geothermal reservoirs, is reasonably well suited for optimization.

The formulation of the objective function was based on an analytical thermal transport model, as well as a correlation between the specific power output and temperature. The specific power output function provided a natural way to incorporate a penalty for falling below a certain minimum design temperature. This made it possible to determine the absolute optimal values of the injection rates for each well, and all the wells combined.

The application of the optimization method to two test cases shows that it works well. The first case is a relatively simple discrete fracture model with two injectors and two producers (Example I). The second case is a more complicated model based on observations from the Soultz-sous-Forêts enhanced geothermal system in France (Example II).

As for any modeling problem, the quality of the results depends greatly on the accuracy of the characterization methods, and as such the results in Example I are more accurate. The optimal flow rate configuration for Example II also yielded quite satisfactory results. These methods are most applicable in fractured reservoirs where there are relatively few dominant flow paths connecting the wells and the reservoir fluid is in the liquid phase. Some of the required data can be obtained by standard methods, while others are relatively hard to obtain. The largest uncertainty probably lies in the estimate of the effective fracture aperture or heat transfer area for each injector–producer pair.

Acknowledgements

This research was conducted with financial support to the Stanford Geothermal Program from the US Department of Energy under grant DE-FG36-08GO18192, the contribution of which is gratefully acknowledged. Motivation and support from Landsvirkjun Power is also gratefully acknowledged.

We would also like to thank Joachim Place and Judith Sausse for providing data to us for building the Soultz flow model.

Finally, we would like to express our gratitude to Golder Associates and DHI-WASY for granting academic licenses for the FRACMAN and FEFLOW software packages, respectively.

References

Albertoni, A., Lake, L., 2002. SPE 75225: Inferring interwell connectivity from well-rate fluctuations in waterfloods. In: Proceedings of SPE/DOE Improved Oil Recovery Symposium, Society of Petroleum Engineers, Tulsa, OK.

Barelli, A., Cappetti, G., Stefani, G., 1995. Exploitation strategy at Laderello Valle Secolo. In: Proceedings of World Geothermal Congress, Kyushu-Tohoku, Japan, pp. 1779–1783.

Bennett, K., Horne, R.N., 2011. Power generation potential from coproduced fluids in the Los Angeles Basin. Geothermal Resources Council Transactions 35, 85–89.

Bodvarsson, G., Pruess, K., 1984. Thermal effects of reinjection in geothermal reservoirs with major vertical fractures. Journal of Petroleum Technology 36, 1567–1578.

Boyd, S., Vandenberghe, L., 2004. Convex Optimization. Cambridge University Press, Cambridge, UK, pp. 701 pp.

Cardoso, M.A., Durlofsky, L.J., Sarma, P., 2009. Development and application of reduced-order modeling procedures for subsurface flow simulation. International Journal for Numerical Methods in Engineering 77, 1322–1350.

DHI-WASY, 2010. FEFLOW 6: User Manual. Berlin, Germany, 116 pp.

Dinh, A.V., 2009. Interwell Connectivity Tests in Waterflood Systems. University of Oklahoma, Norman, Oklahoma, 247 pp. (Ph.D. thesis). Available on the world wide web at http://mpge.ou.edu/research/documents/AnhVDinhDissertation.pdf

Echeverria Ciaurri, D., Isebor, O.J., Durlofsky, L.J., 2011. Application of derivative-free methodologies to generally constrained oil production optimisation problems. International Journal of Mathematical Modelling and Numerical Optimisation 2, 134–161.

Ganefianto, N., Stimac, J., Azwar, L.S., Pasikki, R., Parini, M., Shidartha, E., Joeristanto, A., Nordquist, G., Riedel, K., 2010. Optimizing production at Salak Geothermal Field, Indonesia, through injection management. In: Proceedings of World Geothermal Congress, Bali, Indonesia, 7 pp.

Genter, A., Goerke, X., Graff, J., 2010. Current status of the EGS Soultz geothermal project (France). In: Proceedings of World Geothermal Congress, Bali, Indonesia, 6 pp.

Gringarten, A.C., Sauty, J.P., 1975. A theoretical study of heat extraction from aquifers with uniform regional flow. Journal of Geophysical Research 80, 4956–4962.
Gringarten, A.C., Witherspoon, P., 1975. Theory of heat extraction from fractured hot dry rock. Journal of Geophysical Research 80, 1120–1124.
Jansen, J., 2011. Adjoint-based optimization of multi-phase flow through porous media – a review. Computers & Fluids 46, 40–51.
Juliusson, E., 2012. Characterization of Fractured Geothermal Reservoirs based on Production Data. Stanford University, Palo Alto, California, 264 pp. (Ph.D. thesis). Available on the world wide web at http://pangea.stanford.edu/ERE/pdf/pereports/PhD/Juliusson2012.pdf
Juliusson, E., Horne, R.N., Sweeney, J., Hart, M., Rich, J., Sandler, J., 2011. Optimal extraction of geothermal resources. Geothermal Resources Council Transactions 35, 1457–1466.
Kocabas, I., 2005. Geothermal reservoir characterization via thermal injection backflow and interwell tracer testing. Geothermics 34, 27–46.
Lauwerier, H.A., 1955. The transport of heat in an oil layer caused by the injection of hot fluid. Applied Scientific Research 5, 145–150.
Lee, K.H., 2010. Investigating Statistical Modeling Approaches for Reservoir Characterization in Waterfloods from Rates Fluctuations. University of Southern California, Los Angeles, California, 128 pp. (Ph.D. thesis). Available on the world wide web at http://digitallibrary.usc.edu/cdm/compoundobject/collection/p15799coll127/id/417046/rec/18
Lee, K.H., Ortega, A., Jafroodi, N., Ershaghi, I., 2010. SPE 132625: A multivariate autoregressive model for characterizing producer relationships in waterfloods from injection/production rate fluctuations. In: Proceedings of SPE Western Regional Meeting, Anaheim, CA, p. 11 pp.
Lovekin, J., Horne, R.N., 1989. Optimization of injection scheduling in geothermal fields. In: Proceedings of the Geothermal Program Review VII, pp. 45–52.
Macario, M., 1991. Optimizing Reinjection Strategy in Palinpinon, Philippines based on Chloride Data. Stanford University, Palo Alto, CA, 177 pp. (MS thesis). Available on the world wide web at http://pangea.stanford.edu/ERE/pdf/pereports/MS/Urbino(Macario)91.pdf
Massart, B., Paillet, M., Henrion, V., Sausse, J., Dezayes, C., Genter, A., Bisset, A., 2010. Fracture characterization and stochastic modeling of the granitic basement in the HDR Soultz Project (France). In: Proceedings of World Geothermal Congress, Bali, Indonesia, 7 pp.
MathWorks, 2012. MathWorks fmincon – find minimum of constrained nonlinear multivariable function – MATLAB, From http://www.mathworks.se/help/optim/ug/fmincon.html (retrieved 15.11.12).
Place, J., Garzic, E.L.E., Geraud, Y., Diraison, M., Sausse, J., 2011. Characterization of the Structural control on fluid flow paths in fractured granites. In: Proceedings of Thirty-Sixth Workshop on Geothermal Reservoir Engineering, Stanford University, Stanford, CA, USA, 11 pp.
Reimus, P.W., Watson, T., Vermeul, V., Newell, D., Williams, M., 2011. Laboratory testing and modeling to evaluate perfluorocarbon compounds as tracers in geothermal systems. In: Proceedings of Thirty-Sixth Workshop on Geothermal Reservoir Engineering, Stanford University, Stanford, CA, USA, 9 pp.
Sarma, P., Durlofsky, L., Aziz, K., Chen, W., 2006. Efficient real-time reservoir management using adjoint-based optimal control and model updating. Computational Geosciences 10, 3–36.
Shewchuk, J.R., 1996. Triangle: engineering a 2D quality mesh generator and Delaunay triangulator. Lecture Notes in Computer Science 1148, 203–222.
Shook, G.M., 2001. Predicting thermal breakthrough in heterogeneous media from tracer tests. Geothermics 30, 1–7.
Shook, G.M., 2003. A simple, fast method of estimating fractured reservoir geometry from tracer tests. Geothermal Resources Council Transactions 27, 407–411.
Shook, G.M., 2004. Estimating Fracture surface areas from tracer tests: mathematical formulation. Geothermal Resources Council Transactions 28, 627–630.
Sullera, M.M., Horne, R.N., 2001. Inferring injection returns from chloride monitoring data. Geothermics 30, 591–616.
Tester, J., Anderson, B., Batchelor, A., Blackwell, D., DiPippo, R., Drake, E., Garnish, J., Livesay, B., Moore, M., Nichols, K., 2006. The Future of Geothermal Energy. Impact of Enhanced Geothermal Systems on the United States in the 21st Century.
Wu, X., Pope, G., Shook, G.M., Srinivasan, S., 2008. Prediction of enthalpy production from fractured geothermal reservoirs using partitioning tracers. International Journal of Heat and Mass Transfer 51, 1453–1466.
Yousef, A., Gentil, P., Jensen, J., Lake, L., 2005. SPE 95322: A capacitance model to infer interwell connectivity from production and injection rate fluctuations. SPE Reservoir Evaluation & Engineering 9 (6), 630–646.